

Equilibrium properties of the fluxoid lattice in single-crystal niobium. II. Small-angle neutron-diffraction measurements

D. K. Christen, H. R. Kerchner, S. T. Sekula, and P. Thorel*

Solid State Division, Oak Ridge National Laboratory, Oak Ridge, Tennessee 37830

(Received 30 April 1979)

A small-angle neutron-diffraction technique has been used to measure several properties of the flux-line lattice (FLL) in a single-crystal sphere of pure niobium. For applied fields parallel to several crystallographic directions in the (100) and (1 $\bar{1}$ 0) planes, the low-field mixed state and intermediate mixed state were investigated. From these results, the orientation dependence of the low-field critical parameters H_{c1} and B_0 are deduced. The consistency of these results is verified by comparison with direct measurements of the equilibrium misalignment angle between the applied-field direction and the fluxoid axes. In addition, results are reported which extend the available information concerning correlations between the FLL and crystal lattice (CL) symmetry properties.

I. INTRODUCTION

In the preceding paper,¹ hereafter referred to as I, we presented the results of a thorough study of the equilibrium mixed state of pure niobium using a precise bulk-magnetization technique. In this paper, these results are verified and extended in the low-field regime by a systematic study that employs small-angle neutron scattering, a technique which enables investigation of the flux-line lattice (FLL) on a microscopic level. The present double-crystal small-angle neutron-scattering (DCSANS) technique² is of an unconventional nature, utilizing two identical, perfect crystals of silicon, one to monochromate the beam, and the other to detect the neutrons scattered from the FLL. While sacrificing beam intensity, the procedure enables very high resolution in determining the interfluxoid spacing (or more specifically, the FLL basic-cell area A_c). Then, by virtue of flux quantization, the microscopic average flux density of the FLL can be probed with great precision.

Previous studies have demonstrated the quantitative capability of DCSANS in exploring the properties of a less-reversible niobium sphere at low-to-moderate fields and temperatures, where the microscopic FLL field modulation is large enough to result in sufficient diffracted intensity.² There it was shown that, despite some bulk magnetic hysteresis, there exists a microscopically sharp transition between the intermediate mixed state (IMS) and the mixed state. This was manifested by a well-defined applied-field value $H_2 = \frac{2}{3}H_{c1} + \frac{1}{3}B_0$, below which the FLL basic-cell area A_{c0} was nearly independent of applied field. This FLL basic cell yields the equilibrium flux density $B_0 = \phi_0/A_{c0}$, due to the attractive fluxoid interaction pervasive in the IMS. Here, $\phi_0(2.07 \times 10^{-7} \text{ G cm}^2)$ is the quantum of magnetic flux possessed by each FLL basic cell.

Because of the above properties, DCSANS can be used to resolve the anisotropy in the basic parameters B_0 and H_{c1} for the nearly reversible sample Nb-1 described in I.³ Moreover, these anisotropic properties also manifest themselves as an equilibrium misalignment between the fluxoid axes and the applied field for field directions off high-symmetry crystal-lattice (CL) axes. By employing a scattering geometry sensitive to this effect, direct measurements of the phenomenon can be made.⁴ Finally, information can be obtained regarding the correlation between the FLL and CL symmetry properties.^{5,6}

In the following, the experimental results for these effects are presented, along with some qualitative details of the mixed-state-IMS transition, where an apparent microscopic supercooling was observed.

As pointed out in I, there has been recent theoretical progress in the description of low-field properties in the isotropic limit, but the generalizations to an anisotropic (cubic) system are as yet incomplete. However, from I it is seen that a thermodynamic analysis can go a long way in relating the origins of anisotropy (as they fundamentally contribute to the free energy) to the observable parameters, and in revealing relationships among these observables.

In order to discuss the results, it is helpful to first point out some details regarding the field region in and near the IMS. The existence of a net attractive interaction between fluxoids necessarily results in some small modification to the thermodynamic description given in I of the vortex state in the IMS field region. This is due to the formation in the IMS of FLL domains which modifies the thermodynamic potential in two ways: (i) Because of the negative interaction energy, fluxoids on the surface of an FLL domain are at a relatively higher energy than those in the bulk. This positive surface energy makes such an FLL domain analogous to a flux domain in a type-I

superconductor. (ii) The magnetic field external to the sample has a slightly different distribution than that of a material possessing the same macroscopic, but microscopically uniform, internal flux density. That is, in the regions where the external field exits from the FLL domains, the field energy is higher, by virtue of a larger local flux density, than would exist if the internal flux density were uniformly distributed. For the case of a sphere, close to the sample the external field energy is no longer effectively that of a magnetic dipole centered in the sample. Similarly to a type-I material in the intermediate state, it is the small energy trade-off in these two contributions that produces the equilibrium domain structure in the IMS.⁷ In addition, this effect may be responsible for some "fine structure" in the applied-field dependence of the transition from the mixed state to the IMS. This point will be discussed below.

Since the total extra energy contained in these two effects depends on the particular domain structure (shape, size, separation, surface area, etc.), it is not necessarily proportional to the volume of the sample. Therefore, one must consider a total free energy, rather than a free-energy density, of the system.

For a sphere, it is straightforward to show that Eq. (1) of I can be re-expressed to include the above effects. Written in terms of the applied field \bar{H}_a , it is given by

$$G = V_s \left[-\frac{H_c^2}{8\pi} + \frac{3}{2} \frac{H_a^2}{8\pi} + \frac{\bar{B}}{4\pi} (\bar{H}_{c1} - \frac{3}{2} \bar{H}_a) + \frac{B^2}{16\pi} + \frac{1}{2} \rho C_L \left(\frac{b - B_0}{B_0} \right)^2 \right] + U \quad (1)$$

This is a general expression, valid in the IMS, for a spherical sample of volume V_s . The bulk flux density \bar{B} is defined as $\bar{B} = \rho \bar{b}$, where ρ is the volume fraction of sample occupied by FLL of unit-cell average flux density $b = \phi_0/A_c$. The last term in brackets provides that the FLL lattice spacing may be slightly different from that which defines B_0 (and H_{c1}), with C_L being the FLL compressibility modulus. The quantity U represents the small domain energy terms discussed above. That is, $U = U_\sigma + U_B$, where U_σ and U_B are the domain-wall energy and exterior field energy terms, respectively. U is explicitly a function of \bar{b} and ρ and implicitly a function of the size and shape distributions of the domains. It can be seen that $G = G(\bar{b}, \rho)$ in the IMS. Equation (1) neglects contributions to G due to field-dependent changes in the FLL symmetry structure. This is justified by the experimental fact that, at fixed sample orientation, the observed FLL symmetry is independent of field in the IMS. With $U = 0$ and $\rho = 1$, Eq. (1) is also valid for small applied-field excursions into the mixed state. It is worth pointing out that the intrinsic parameter H_{c1} in Eq. (1) is defined as

$\bar{H}_{c1} = 4\pi \nabla_{\bar{B}} f|_{B_0}$ in terms of the free-energy density f [Eq. (3) of I for an infinite medium]. In general,

$$\nabla_{\bar{B}} = \hat{b}(\rho^{-1} \partial/\partial b + b^{-1} \partial/\partial \rho) + B^{-1} \nabla_b;$$

for an infinite material $\rho = 1$, $b = B$, and the second term in parentheses does not contribute.

To the extent that U is completely negligible, the minimization of Eq. (1) predicts that ρ varies linearly in the applied-field range $\frac{2}{3} H_{c1} \leq H_a \leq H_2$. The flux density per FLL unit cell is found to be fixed at $b = B_0$; thus the bulk flux density is $\bar{B} = \rho \bar{B}_0 = 3(\bar{H}_a - \frac{2}{3} \bar{H}_{c1})$ in the IMS. However, for applied fields slightly below H_2 , full account of U in the minimization procedure is straightforward and yields an interesting result. For $H_a = H_2 + \delta H_a$, one obtains

$$\rho = 1 + \frac{3\delta H_a}{B_0} + \left[\frac{\partial U}{\partial[(b - B_0)/B_0]} - \left(1 + 8\pi \frac{C_L}{B_0^2} \right) \frac{\partial U}{\partial \rho} \right] / C_L V_s$$

Now, for ρ infinitesimally less than unity, it can be argued that the quantity in brackets is positive⁸, so the equilibrium transition to a "domain-characterized" IMS (i.e., $\rho < 1$) occurs at an applied field H_2^* slightly less than H_2 ,

$$H_2^* = H_2 - \frac{B_0}{3C_L V_s} \times \left[\frac{\partial U}{\partial[(b - B_0)/B_0]} \Big|_{\rho=1} - \left(1 + \frac{8\pi C_L}{B_0^2} \right) \frac{\partial U}{\partial \rho} \Big|_{\rho=1} \right]$$

Moreover, at $H_a = H_2^*$,

$$B = b = B_0 \left[1 - \frac{(H_2 - H_2^*)}{\frac{1}{3} B_0} \left(1 + \frac{8\pi C_L}{B_0^2} \right)^{-1} \right]; \quad (2)$$

that is, as H_a is decreased from the mixed state, the flux density per unit cell b has a value slightly below B_0 as the domains just appear, and it is this phenomenon which may appear as a supercooling of the mixed state. As mentioned above, a detailed analysis of $\bar{B}(\bar{H}_a)$ for $\rho < 1$ must be obtained from a particular model for $U(\bar{b}, \rho)$ and minimization of $G(\bar{b}, \rho)$. These details will be explored elsewhere.⁸

Within the IMS, where it is expected that $\bar{B} = \rho \bar{B}_0$, the condition $\nabla_{\bar{B}} G = 0$ implies

$$\bar{B} = 3\bar{H}_a - 2\bar{H}_{c1} - \frac{8\pi \nabla_{\bar{B}} U}{V_s}, \quad (3)$$

which determines \bar{B} implicitly. Equation (3) is equivalent to the combination of Eqs. (9) and (10) of I for $H = H_{c1}$, and in the limit $U \rightarrow 0$.

A minimization of the Gibbs potential, Eq. (1), with respect to virtual rotations of the fluxoids within the material (the condition $\nabla_{\hat{b}}G=0$) yields the equilibrium misalignment angle $\Delta\psi$ between \vec{B} and \vec{H}_a in the IMS,

$$\sin \Delta\psi H_a = -\frac{2}{3} \frac{\partial(\hat{B}_0 \cdot \vec{H}_{c1})}{\partial \Delta\psi} - \frac{8\pi}{V_s B} \partial U / \partial \Delta\psi \quad (4)$$

Since the microscopic parameters that determine the value of H_{c1} (i.e., those parameters which determine the core and interaction energies of the FLL system) are functions of the FLL-CL orientation, it results that

$$\frac{\partial(\hat{B}_0 \cdot \vec{H}_{c1})}{\partial \Delta\psi} = \frac{d(\hat{B}_0 \cdot \vec{H}_{c1})}{d\alpha} \left[1 + \frac{d\Delta\psi}{d\alpha} \right]^{-1}$$

Here, α is the angle (in a CL reflection plane) specifying the orientation of the CL with respect to the applied field. Thus, the variation of the material-dependent quantity $(\hat{B}_0 \cdot \vec{H}_{c1})$ with respect to rotations of the fluxoids inside the medium is equivalent to that with respect to rotations of the sample in the external field H_a , to within a factor $(1 + d\Delta\psi/d\alpha)^{-1} \approx 1$. Furthermore,

$$\sin \Delta\psi H_a \approx -\frac{2}{3} H_{c1} \frac{(dH_{c1}/d\alpha)}{H_{c1}} + \frac{4\pi C_L}{3B_0} \left[\frac{B - B_0}{B_0} \right] \left[\frac{2(dB_0/d\alpha)}{B_0} - \frac{B_0}{B} \left[\frac{B - B_0}{B_0} \right] \frac{(dC_L/d\alpha)}{C_L} \right] \quad (6)$$

Then, the (low-field) mixed-state misalignment is given in terms of the relative anisotropies in H_{c1} , the FLL compressibility modulus C_L , and in the flux density B_0 . Equation (6) should be valid to the extent that the fluxoid interaction is harmonic, and there is no FLL orientation change over the (small) applied-field excursion into the mixed state.

Correlations of the FLL basic-cell orientation and shape with respect to the CL symmetries have been investigated previously, both experimentally and theoretically, over limited ranges of the temperature-field-orientation space, and these results were reviewed by Schelten.⁵ The theories seek to relate the FLL morphology to anisotropies in the microscopic superconducting and normal-state parameters, through a minimization of the free energy.⁹⁻¹² For the most part, the range of validity is limited to near H_{c2} , where it is difficult to observe the FLL either by neutron diffraction or by electron microscopy. At lower flux densities, where the experiments are done, the observed behavior appears to be in reasonable agreement with the high-field theory in Nb, except for applied fields near to fourfold CL axes. In this latter case, theory fails even qualitatively, where experiments reveal two or more domains of FLL, with different orientation, to coexist in the sample.

The present experimental results extend the avail-

$d(\hat{B}_0 \cdot \vec{H}_{c1})/d\alpha = dH_{c1}/d\alpha$ to the same order of approximation. The second term in Eq. (4) involves the small domain energies, and is neglected in the experimental analysis of the misalignment angle described below. Thus,

$$\Delta\psi \approx \frac{\frac{2}{3} H_{c1}}{H_a} \left[\frac{dH_{c1}/d\alpha}{H_{c1}} \right]; \quad (5)$$

and it is seen that $\Delta\psi$ is related to the relative anisotropy in H_{c1} and is inversely proportional to the applied field in the IMS. It has been pointed out previously that the simple thermodynamic relation Eq. (5) enables determination of relative H_{c1} anisotropy by means of a torque experiment (or direct measurement of $\Delta\psi$ by neutron scattering).⁴ In the case of an IMS torque density measurement, one deduces $dH_{c1}/d\alpha$ from the relation $\tau \approx B(dH_{c1}/d\alpha)/4\pi$, which also requires independently ascertaining the bulk flux density B .

For small field excursions into the mixed state, where the fluxoids become more compressed by the external applied-field "pressure," Eq. (1) applies for $\vec{b} = \vec{B}$, $\rho = 1$, and $U = 0$. In this case, the misalignment angle, given by the condition $\nabla_{\hat{b}}G = 0$, is slightly more complicated,

able data, as we report the variation of the FLL basic-cell orientation and shape: (i) for applied fields parallel to several CL axes and in the $(1\bar{1}0)$ and (100) planes at constant temperature 4.30 K, in the IMS. Emphasis is placed on ascertaining at which orientations multiple FLL domains may exist; (ii) for higher-field intensity in the mixed state; (iii) for various temperatures between 1.5 and 7.5 K, in the IMS, for the three high-symmetry CL axes $\langle 111 \rangle$, $\langle 110 \rangle$, and $\langle 100 \rangle$.

In the following, Sec. II is devoted to a brief description of the DCSANS experimental technique, and the role of the particular experimental geometries used for the anisotropy measurements of B_0 , H_{c1} , and the FLL morphology, and for the determinations of the FLL-applied-field misalignments. In Sec. III, the experimental results are presented and discussed in relation to the other available data and the current state of the theory.

II. EXPERIMENTAL METHOD

The DCSANS experimental arrangement is shown schematically in Fig. 1. The horizontal neutron beam, which is monochromated to a mean wavelength $\lambda = 2.59 \text{ \AA}$ by Bragg scattering from the

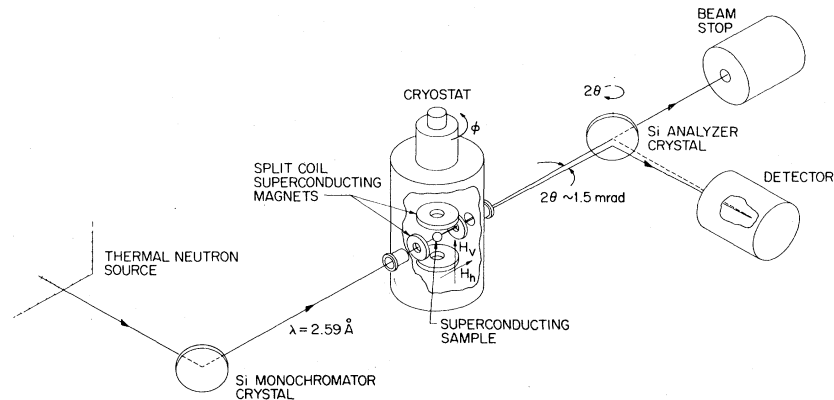


FIG. 1. Schematic representation of the double (silicon)-crystal small-angle neutron-scattering (DCSANS) apparatus. H_h or H_v represents either horizontal or vertical magnetic fields applied by split-coil superconducting magnets.

first perfect silicon crystal, passes through aluminum windows and the sample located in the inner, rotatable section of the cryostat. Either a horizontal or vertical magnetic field may be applied to the sample by means of two orthogonal split-coil superconducting magnets. Neutrons that are Bragg scattered from a given set of FLL planes deviate from the direct beam by a small angle 2θ . These scattered neutrons can be detected by rotating the silicon analyzer crystal (which is identical to the monochromator crystal) about a vertical axis until the FLL scattered neutrons are in Bragg reflection from the analyzer crystal, and then are diffracted into the (fixed) detector. The angular difference between the position of the analyzer crystal for Bragg reflection from the (hk) FLL planes

and reflection of the direct (undeviated) neutron beam is simply related to the scattering angle $2\theta_{hk}$. This can be seen in Fig. 2, which shows schematically the scattering situation in reciprocal space. In Fig. 2 (a) is the case when the applied magnetic field H_a is vertical ($\vec{H}_a = \hat{y}H_a$). If the fluxoids are perfectly parallel to \vec{H}_a , then the two-dimensional FLL reciprocal lattice lies in the horizontal x - z plane. The Bragg condition is satisfied when the surface of the Ewald sphere (of radius $k_0 = 2\pi/\lambda$ centered at the origin of incident neutron wave vector \vec{k}_0) intersects a reciprocal-lattice point \vec{G}_{hk} of the FLL [(hk) = (10) for the illustration of Fig. 2]. The scattering vector then lies along the x axis of Fig. 2(a) and is given in terms of the measured angle $2\theta_{hk}$ by $G_{hk} = k_0 2\theta_{hk}$.

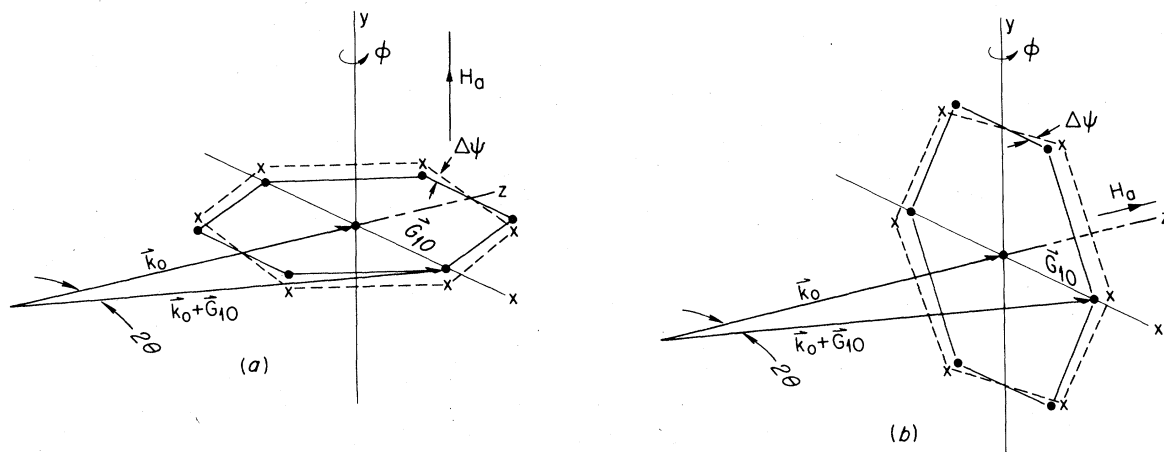


FIG. 2. Reciprocal-space representation of: (a) Diffraction geometry when a vertical magnetic field H_a is applied, resulting in an FLL reciprocal lattice (●) which lies in the horizontal plane for the case of no misalignment. Misalignment between FLL and H_a results in reciprocal points represented by (×). (b) Diffraction geometry when a horizontal field H_a produces FLL. The lowest-order (10) Bragg reflection is shown for the case of no misalignment (●). When misalignment occurs (×), the FLL reciprocal space must be rotated about a vertical axis through the angle $\Delta\psi$ in order to achieve the Bragg condition.

Rotation of the sample through the angle ϕ about the vertical y axis brings into Bragg reflection FLL planes of any chosen (hk) . From this, one may ascertain the symmetry of the FLL and the area of an FLL reciprocal-lattice basic cell A_c^* . This is related to the FLL unit-cell area A_c in real space according to $A_c = A_c^*/(2\pi)^2$, which yields the average flux density per unit cell, $b = \phi_0/A_c$. The quantity b ascertained in this way should agree with bulk-magnetization measurements to the extent that the FLL is in true thermodynamic equilibrium, possesses few lattice "defects," and completely fills the material (this latter condition is not satisfied in the IMS).

In an anisotropic superconductor the fluxoids, in general, will be straight, but slightly nonparallel to the applied field \vec{H}_a . This situation is illustrated in Fig. 2(a) by the dashed reciprocal-lattice cells. In this case, the scattering vector will lie in the x - y plane, but may be off the x axis. (Note: Since $k_0/G_{10} \approx 750$, the Ewald sphere is essentially a plane over the reciprocal-space area of interest.) Because of the optics of the double-crystal apparatus, the analyzer crystal effectively integrates all scattered intensity along a vertical strip in reciprocal space, the width of which is given by the resolution of the instrument, and the height by the vertical collimation of the beam. Therefore, it is the vector projection of the scattering point onto the x axis which is detected by rotation of the analyzer crystal. Thus, for the case of a misalignment angle $\Delta\psi$ between the fluxoids and the applied field, the measured cell area in reciprocal space A_c^{**} is given in terms of the actual cell area A_c^* according to $A_c^{**} = A_c^* \cos \Delta\psi$. Consequently, a general cell-area measurement using the vertical applied-field configuration yields the quantity

$$\vec{b} \cdot \vec{H}_a = \phi_0(\cos \Delta\psi)/A_c \approx \phi_0/A_c \quad ,$$

since typically $\Delta\psi < 1^\circ$.⁴

For illustration, the typical angular separation between the direct beam 2θ peak and a (10) FLL Bragg peak at $T = 4.3$ K, and in the IMS field regime, is about 350 arcsec (1.69 mrad), corresponding to a scattering vector of magnitude $4.12 \times 10^{-3} \text{ \AA}^{-1}$. For a typical 2θ -peak width of about 6-arcsec full width at half maximum, the centroid of the peak can be determined to a precision ± 0.2 arcsec. In practice, the angle $4\theta_{hk}$ is found by relative measurement of the FLL (hk) and $(\bar{h}\bar{k})$ 2θ peaks. Following this procedure for three successive lowest-order Bragg reflections, the FLL unit-cell area can be determined to about 0.1% precision.

It should be pointed out that, in principle, the most precise determination of the FLL cell area should come from observing the highest-possible-order Bragg reflections, where the 2θ separation would be largest. In practice, however, the scattered intensity from any reflections of higher order than first is very

small. This results because the integrated scattered intensity is given by²

$$I_{hk} \propto \frac{|h_{hk}|^2}{G_{hk}} \quad .$$

Here, h_{hk} is the form factor for the microscopic flux density distribution within an FLL unit cell,

$$h_{hk} = \frac{1}{A_c} \int d^2\vec{r} e^{i\vec{G}_{hk} \cdot \vec{r}} h(\vec{r}) \quad .$$

So, not only is the intensity inversely proportional to the magnitude of the reciprocal vector, but it is known that $h_{11}/h_{10} \approx 10^{-1}$ for niobium at low flux densities,¹³ yielding $I_{11}/I_{10} \approx 10^{-2}$. Thus, the trade-off between 2θ resolution and counting time dictated that the lowest-order reflections be used.

As noted previously,³ the FLL Bragg peaks are always slightly broader than the direct peak, but at present no attempt has been made to derive conclusions regarding the FLL long-range coherence, or interplanar spacing distribution. The reason for this is due to decorrelating effects between neutron rays from monochromator to analyzer, which intrinsically result from the small-angle scattering from the sample. Thus, some broadening is expected, even for "ideal" Bragg conditions in the FLL, and a separation of these effects would have to be made for a detailed interpretation.

While the vertical applied-field configuration is useful for determination of anisotropy in the FLL symmetry and cell area (flux density), the horizontal-field situation can be employed for direct observation of the fluxoid-applied-field misalignment.⁴ The reciprocal-space illustration of this is in Fig. 2(b), while the real-space-measurement procedure is depicted schematically in Fig. 3. In this case, rotation of the cryostat inner section through the angle ϕ rotates both the sample and the horizontal magnet as a unit. Thus, FLL reciprocal-lattice points that are off the Ewald sphere surface [the x - y plane of Fig. 2(b)] due to misalignment can be brought into the Bragg condition by rotation about the vertical axis by an angle $\phi = \Delta\psi$, the misalignment angle. As shown in Fig. 3, the zero of $\Delta\psi$ is established by orienting the sample inside the horizontal magnet such that the field is parallel to a high-symmetry niobium crystallographic direction, for which the misalignment angle is zero. Then, misalignment angles can be studied systematically for fields parallel to various CL directions in a fixed (horizontal) CL plane. This is accomplished by measuring the shift in the so-called ϕ -rocking-curve peak positions for various fixed sample orientations.

The chosen CL plane in which the misalignment angles are studied must be a reflection plane of the CL. In this way, the FLL misalignments will occur only in the horizontal plane [as illustrated in Fig. 2(b) and Fig. 3]. Otherwise, the previously described

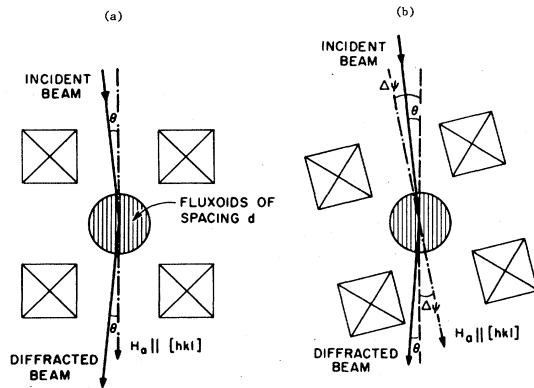


FIG. 3. Schematic real-space top view of the scattering geometry used to measure the misalignment angle. (a) Special case where $[hkl]$ is a high-symmetry CL axis. Here the fluxoids are parallel to \vec{H}_a , and the Bragg angle is $\theta = \lambda/2d$, for neutron wavelength λ . (b) $[hkl]$ is low-symmetry direction, and the misalignment angle lies in the horizontal plane (plane of figure), which is a CL reflection plane. Here the fluxoids are nonparallel to H_a , and the entire magnet-sample assembly must be rotated by $\Delta\psi$ in order to preserve the Bragg condition.

vertical integrating feature of the double-crystal diffractometer renders it difficult to properly interpret a general misalignment direction.

Most of the studies described in the following were performed at $T = 4.30$ K for magnetic fields applied parallel to several CL directions in both the $(1\bar{1}0)$ and (100) planes. The sample used was the same large, single-crystal sphere of pure niobium which is described in detail in I (the FLL morphology data also include some results for a second sample, Nb-2). For the vertical (horizontal) field configurations, the sample could be oriented *in situ* by rotation about a single, well-defined horizontal (vertical) CL axis. This axis (either a $\langle 100 \rangle$ or $\langle 110 \rangle$) was found externally, prior to sample insertion into the cryostat, by x-ray Laue backscattering, in a manner similar to that described in I. In the cryostat, the sample was suspended on an Al mounting post, sitting in helium exchange gas inside an aluminum chamber.

Temperature was measured by means of a calibrated Ge resistance thermometer, while temperature stability was facilitated by an electronic temperature controller, which regulated the aluminum-sample-chamber temperature to ± 0.002 K at $T = 4.30$ K for time periods of several hours.

In order to clarify the technique employed here, it is helpful to observe what one measures with DCSANS for a given sample orientation at fixed temperature. In Fig. 4, we illustrate an idealized flux-density-applied-field relationship, given by the solid curve, for a spherical specimen, compared to the actual average flux density per FLL unit cell, as measured by DCSANS.

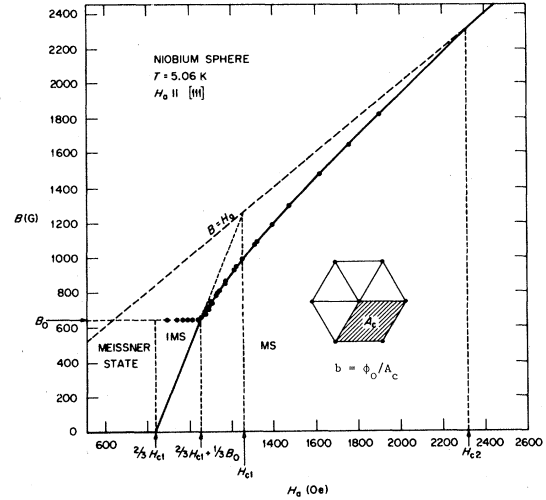


FIG. 4. Idealized bulk flux density B (solid curve) vs applied field H_a for a niobium sphere at $T = 5.06$ K, compared to the experimental average flux density per FLL unit cell b obtained from DCSANS. The inset shows how the flux density per unit cell is found from the flux-quantum condition.

The microscopic transition which occurs at the applied field $H_2 = \frac{2}{3}H_{c1} + \frac{1}{3}B_0$ is very sharp and can be detected easily by DCSANS using the following technique. For a given low-order reflection, the diffractometer analyzer crystal is set to diffract at the $2\theta_0$ angle corresponding to the IMS-FLL. The scattered-neutron intensity is then recorded as the applied field H_a is stepped from the MS to the IMS, or vice versa. The position of peak intensity is the applied-field boundary H_2 between the MS and IMS, and typically it may be determined to a precision ± 1 Oe. In the IMS, the field dependence of scattered intensity is nearly linear, due to the volume-filling-fraction effects.

Since B_0 is determined independently by the FLL cell-area measurement in the IMS, one may use the value of $H_2 = \frac{2}{3}H_{c1} + \frac{1}{3}B_0$ to calculate

$$H_{c1} = \frac{3}{2}(H_2 - \frac{1}{3}B_0) . \quad (7)$$

It is for this procedure that perfection in the sample geometry is important. For near-spherical spheroidal geometry, the demagnetizing factor is given by $D = \frac{1}{3}(1 - \epsilon^2)$, where ϵ is the eccentricity (zero for a sphere). Then, using the technique described above, the possible error in H_2 due to geometry alone is, $\Delta H_2 = \pm \frac{1}{3}\epsilon^2(H_{c1} - B_0)$, where H_{c1} is the true lower critical field of the material. Thus, the error in the H_{c1} value derived from Eq. (7) would be $\Delta H_{c1} = \pm \frac{1}{2}\epsilon^2(H_{c1} - B_0)$. For example, at $T = 4.30$ K, where $H_{c1} = 1429$ Oe and $B_0 = 748$ G, the maximum eccentricity $\epsilon = 0.035$ of Nb-1 yields a possible geometrical error in the H_{c1} determination of ± 0.4 Oe.

III. RESULTS AND DISCUSSION

A. Details of IMS-mixed-state transition

In Sec. I we mentioned an apparent supercooling phenomenon which is observed over a narrow applied-field range just below H_2 . We discuss this effect here briefly since it has bearing on the deduced values of H_{c1} and B_0 .

This effect is best illustrated by observing, on an expanded scale, the DCSANS local flux-density vs applied-field data in a narrow field range about $H_2 = \frac{2}{3}H_{c1} + \frac{1}{3}B_0$. This is shown in Fig. 5(a), along with an associated field scan, Fig. 5(b), described in Sec. II, for the case $H_a \parallel [111]$, and $T = 4.30$ K. In Fig. 5(a), it is seen that, for decreased field history, the flux density per FLL unit cell dips below, before reattaining, that value pervasive throughout the remainder of the IMS. Moreover, no such dip is apparent on increased field. This effect is manifested as a sharp peak in the decreased field scan intensity of Fig. 5(b), owing to the neutron-scattering angle's first attaining, then losing, and then reattaining the IMS value $2\theta_0$ as the applied field is stepped down. (Note: The DCSANS instrument was set up to accept neutrons only at the scattering angle $2\theta_0$ determined at low field in the IMS as described in Sec. II.) The phenomenon is repeatable and apparently static

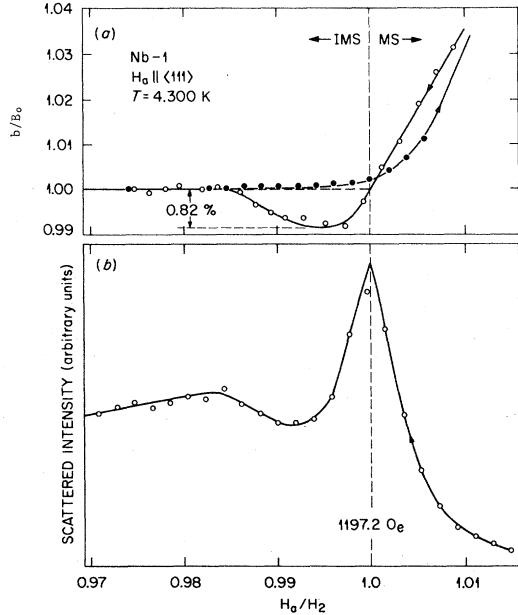


FIG. 5. (a) Expanded view of the reduced flux density per unit cell near the transition from the IMS to mixed state. The FLL undergoes a small expansion (dip in b/B_0) on decreased applied field, which is not present when the field is increased. (b) Scattered neutron intensity for a field scan described in Sec. II. The fields H_2 and B_0 are defined as shown.

(at least for time periods on the order of several minutes required for counting).

It seems most likely that this effect is due to the small energies U , described in Sec. I, which are associated with the formation of domains (most likely Meissner voids in the full FLL) as the field is decreased from the mixed state.^{7,14} A small energy trade-off dictates that it is at first more favorable to expand the FLL than to open holes in it, as described by Eq. (2), while at lower fields the FLL domain structure contribution is relatively much smaller. On increasing field the domain-structure history is different, and may present no "conflict" requiring the expansion. As mentioned previously in Sec. I, in order to quantify this conjecture, one must choose models for the domain structure, and ascertain which conditions minimize the thermodynamic free energy. These details will not be presented here; rather, in view of the excellent reversibility of this specimen throughout the mixed state, we shall assume the phenomenon to be an equilibrium or metastable process (it is difficult to deduce how any form of flux pinning or surface barrier could produce such an effect). Therefore, B_0 is taken to be that field-independent flux density per FLL unit cell which exists throughout the rest of the IMS. Then, the transition field H_2 is found by intersection of the flat B_0 line with the decreased field curve of Fig. 5(a), which is also the applied field of the field-scan intensity peak of Fig. 5(b).

One may note that there exists about a 0.25% maximum hysteresis in the applied-field value in the mixed state, for fields just above H_2 . This effect gradually vanishes for larger applied fields, and most likely poses no problem to the interpretation of H_2 anisotropy, since both the sense and magnitude of the hysteresis are observed to be essentially orientation independent. (Calibration of the split-coil superconducting magnet field versus current relation by means of a Hall probe indicated that at least a part of this apparent history effect can be ascribed to hysteresis in the applied-field magnet.) Moreover, the small FLL expansion and contraction on decreasing field were present at all orientations, and displayed no systematic anisotropy either in magnitude or applied-field breadth to within the experimental resolution.

B. H_{c1} and B_0 anisotropy

Figure 6 illustrates the anisotropy in the measured quantities H_2 and B_0 at $T = 4.30$ K, for fields parallel to several directions in the $(1\bar{1}0)$ and (100) CL planes. The solid curves result from least-squares fits of the data to a series expansion in the orthonormal cubic harmonic functions \mathcal{H}_l , described in I. The curves representing the H_{c1} anisotropy are derived using Eq. (7) applied to the H_2 and B_0 fits, while the

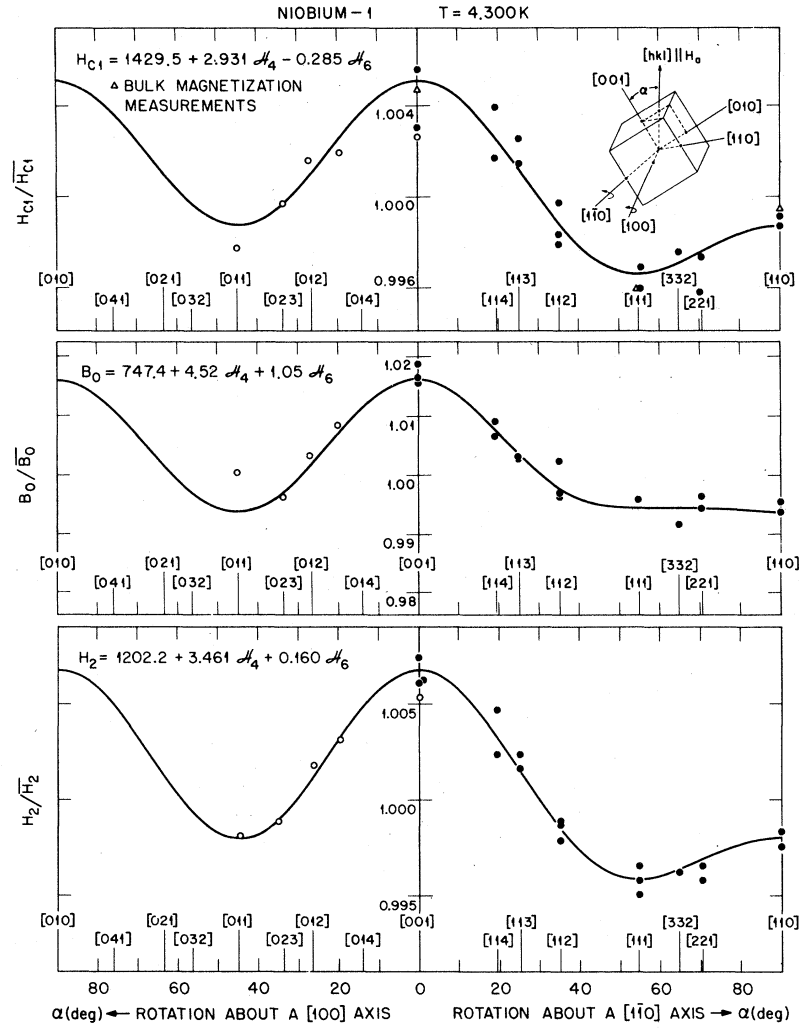


FIG. 6. Experimental data at $T = 4.30$ K for the anisotropy of H_2 , B_0 , and H_{c1} for applied fields in the $(1\bar{1}0)$ and (100) niobium crystal planes. Solid curves are derived from cubic-harmonic fits to the $(1\bar{1}0)$ data.

individual points result from a point-by-point application of the same to the experimental data. Only the data for fields in the $(1\bar{1}0)$ CL plane were used for the numerical fit, allowing comparison of the (100) CL plane data with a curve obtained from expansion coefficients found independently. Favorable agreement in this sense confirms self-consistency of the measurements. Although the anisotropy in B_0 was not resolved by the technique used in I, there is generally good agreement between the two methods for the H_{c1} anisotropy, as shown by the three bulk-magnetization data plotted in Fig. 6. From the fits, one obtains the following results for the relative B_0 and H_{c1} anisotropy at $T = 4.30$ K,

$$\begin{aligned} \Delta B_0/\bar{B}_0 &= 6.05 \times 10^{-3} \mathcal{C}_4 + 1.40 \times 10^{-3} \mathcal{C}_6, \\ \Delta H_{c1}/\bar{H}_{c1} &= 2.05 \times 10^{-3} \mathcal{C}_4 - 1.99 \times 10^{-4} \mathcal{C}_6. \end{aligned} \quad (8)$$

Here, \bar{H}_{c1} and \bar{B}_0 are the orientation-averaged parameters. From these relations, and from inspection of Fig. 6, it is seen that the magnitude of the maximum relative anisotropy is about 1% for H_{c1} and 2% for B_0 , smaller than the effects observed, for example, in H_{c2} and κ_2 which from I are about 5% and 8%, respectively, at this temperature. Although a general low-field theory of anisotropy has not yet evolved, Takanaka and Hubert (TH)¹⁵ have used the Neumann-Tewordt anisotropic generalization of the Ginzburg-Landau equations to show that, near T_c , the relative H_{c1} anisotropy should be smaller than that of H_{c2} , and have the opposite orientation dependence. Both of these qualitative features are in agreement with the present data, as are the preliminary results of a theoretical description of the low-temperature anisotropies in B_0 and H_{c1} , using the bo-

son formalism.¹⁶ From the results of TH, which consider only lowest-order contributions due to the Fermi velocity anisotropy, one obtains for the ratio of the maximum relative anisotropies in H_{c1} and H_{c2} , at T_c ,

$$\frac{\Delta H_{c1}/\bar{H}_{c1}}{\Delta H_{c2}/\bar{H}_{c2}} \approx -0.21.$$

An extrapolation of the TH theory, valid near T_c , to $t = 0.46$, would probably not be useful, since that description of the isotropic part of H_{c1}/H_c displays the wrong temperature dependence (see Sec. III B of Paper I).

The calculation of TH actually applies to the field H_{c1}^* , the idealized superheating field discussed in I, since it treats equilibrium with respect to a single, isolated fluxoid. In I, it was pointed out that the field of first flux penetration H_1 is expected to be more closely associated with the nucleation of isolated fluxoids than is H_2 , which reflects the attractive interaction effects of the fluxoid system. Moreover, the results of I indicate that H_1 displays a different anisotropy than H_2 . Since the observed anisotropy in H_1 could be due to the combined effects of other superheating mechanisms, one cannot construe this observation to refute the results of TH. However, it does point up the need for a theoretical analysis of the anisotropy which fully accounts for the role of the (anisotropic) attractive fluxoid interaction.

Recently, Ohta and Ohtsuka¹⁷ have reported measurements of H_{c1} for niobium and vanadium spheres, which show a different anisotropy than the present results. In the (110) CL plane at 1.8 K, they observed a 1.8% maximum anisotropy, with an absolute minimum of H_{c1} for the applied field parallel to a crystallographic [110], and an absolute maximum at a [001]. Since their technique is a magnetization determination of the field of first flux penetration, it is noteworthy that their results are in qualitative agreement with the present H_1 data of I. Moreover, in contrast to the present H_2 results (and the deduced H_{c1} values) the H_1 anisotropy observed by Ohta and Ohtsuka cannot be fit to a small number of cubic-harmonic functions.

It is possible that an intrinsic property of the superconducting state results in such a complicated anisotropy pattern, but it is presently our opinion that the much-more-reversible transition at H_2 is indicative of H_{c1} defined in a thermodynamic sense. This transition point occurs with the sample full of FLL, under the influence of its full interaction forces, and relatively free of such extrinsic complications as FLL domain size effects and other superheating mechanisms.

Equation (8) and Fig. 6 show that the B_0 anisotropy also can be described by a low-order expansion in cubic harmonics. Recently, Gough¹⁸ has reported measurements of B_0 in niobium using a novel tech-

nique by which the ultrasonic attenuation is recorded as a function of the bulk flux density in the specimen. These results, for $T = 1.8$ K, are in reasonable agreement with the magnitude of the present B_0 data at that temperature. However, Gough deduces that his data display a large 6% relative anisotropy in the (100) CL plane, with the absolute minimum occurring at a [001]. This is in disagreement with the present results which, for temperatures between 1.6 and 4.3 K, show a nearly constant maximum relative anisotropy of about 2% in the (100) plane, with the maximum B_0 occurring for applied fields along a [001] axis. Moreover, Gough's anisotropy pattern possesses a complicated structure that cannot be fit to a small number of cubic harmonics.

It is difficult at this time to speculate on the source of this discrepancy, since the two experimental methods are vastly different. One possible source of difficulty in Gough's procedure, however, involves his reliance on the absence of flux leakage from the sample as it is cooled in a fixed applied field. To assure this, he purposefully damaged the surface of the cylindrical specimen (demagnetizing factor $D = \frac{1}{2}$ in transverse applied field), in order to introduce a strong surface pinning barrier to flux exit. If this is not totally effective, it is possible the observed orientation dependence is an artifact of nonuniform surface pinning and flux distribution. Another possible ambiguity, which could affect the results of both experiments, involves the influence of the FLL domain structure on the flux density within the FLL domains, for the IMS field regime of a sample having a nonzero demagnetizing geometry. The possible ramifications of this effect on the present B_0 measurements were discussed in Sec. III A. Since both the sample geometry and measurement technique are different in Gough's experiments, the phenomenon might affect those observations differently.

C. Misalignment angle between \vec{B} and \vec{H}_a

It was shown by Eq. (5) that an anisotropy in H_{c1} should produce an equilibrium misalignment between the direction of the fluxoid axes \hat{B} and that of the applied field H_a in the IMS.⁴ Moreover, to the extent that the interfluxoid interaction is harmonic for small field excursions into the mixed state, Eq. (6) shows that the misalignment angle $\Delta\psi$ also depends on the anisotropy in B_0 and the FLL compressibility modulus C_L .

The misalignment angle $\Delta\psi$ was measured directly by DCSANS using the horizontal-field geometry described in Sec. II. With this technique, the relative shift in the so-called rocking-curve intensities can yield $\Delta\psi$ to $\pm 0.02^\circ$ at $T = 4.30$ K (the temperature at which all misalignment data were obtained).

In Fig. 7 are experimental data of FLL misalign-

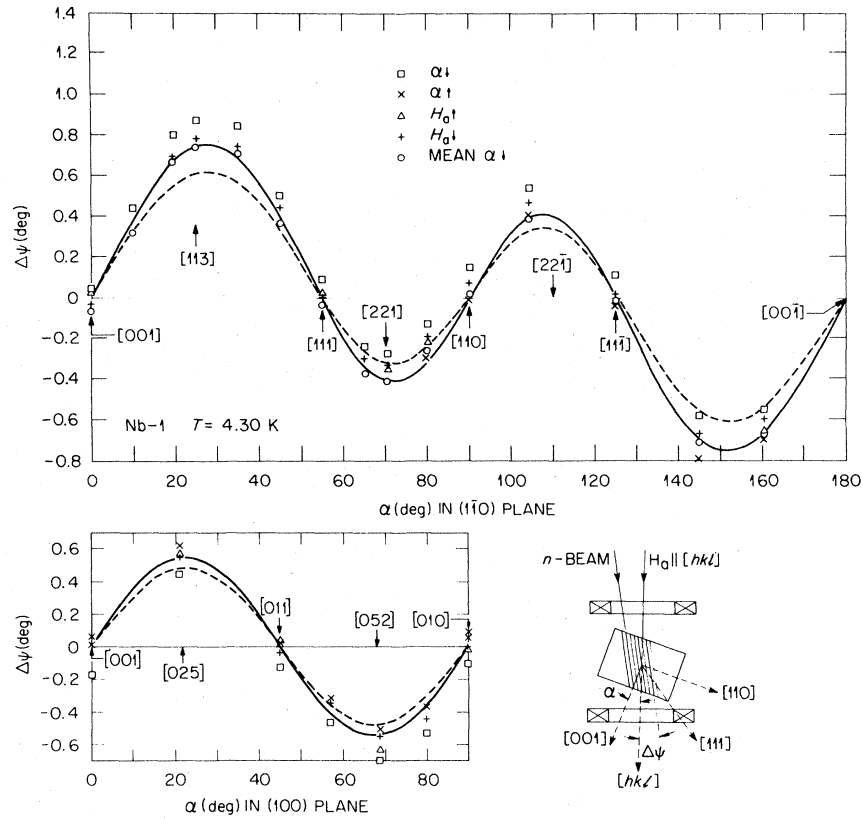


FIG. 7. Misalignment angle $\Delta\psi$ at constant applied field $H_a = 1175$ Oe in the IMS at $T = 4.30$ K, for various field directions in the $(1\bar{1}0)$ and (100) CL planes. The dependence of $\Delta\psi$ on the history of the FLL is shown, where \uparrow (\downarrow) means increased (decreased) to the final value of measurement. The inset shows the top-view geometry and sense of the angles. The systematic dependence on the FLL history was averaged out using the results at equivalent CL directions for the decreased- α case. The solid curve shows the best fit of these data to a series expansion in the angular derivatives of orthonormal cubic-harmonic functions. The dashed line is the misalignment angle deduced from the thermodynamic relation Eq. (5) and the measured H_{c1} anisotropy.

ments in the IMS at fixed $H_a = 1175$ Oe for several applied-field directions in the $(1\bar{1}0)$ and (100) CL symmetry planes. The direction of $\Delta\psi$ is such that the fluxoids are always deviated toward the nearest $\langle 111 \rangle$ CL axis in the $(1\bar{1}0)$ plane, and the nearest $\langle 110 \rangle$ in the (100) plane. In addition, a systematic dependence of $\Delta\psi$ on the history of the FLL was observed, with the largest disparity occurring for histories of opposite rotation of the sample in the fixed applied field. This effect is most likely due to very small remnant bulk or surface flux pinning, which tends to "drag" the fluxoids with the sample when it is in rotational motion. Consequently, the FLL is left with a "memory" of the rotational history after the sample is stopped. This small effect was compensated by averaging the $\Delta\psi$ values for equivalent orientations symmetric about high-symmetry directions.

Since the H_{c1} anisotropy can be fit directly to an expansion in cubic-harmonic functions according to Eq. (8), then the relation Eq. (5) dictates that $\Delta\psi$

should be fit to an expansion in the angular derivatives of cubic harmonics. (Note that the \mathcal{H}_l are functions of only one angle, α , for CL directions lying in a reflection plane.) The results of such a fit to the $(1\bar{1}0)$ $\Delta\psi$ data yield, in units of deg Oe,

$$\Delta\psi H_a = -135 \frac{\partial \mathcal{H}_4}{\partial \alpha} + 14.5 \frac{\partial \mathcal{H}_6}{\partial \alpha} \quad (9)$$

Again, the good representation of the results in the (100) plane using expansion coefficients from the $(1\bar{1}0)$ plane fit points up the consistency of the measurements. The dashed lines of Fig. 7 are the predicted misalignment angles deduced from the measured H_{c1} anisotropy, using Eq. (5). Certainly there is no doubt as to the agreement between the two independent experimental determinations in the sense and structure of the anisotropy. In absolute magnitude, the H_{c1} results fall below the actual measured $\Delta\psi$, but one should keep in mind that the $\Delta\psi$ measurements are a sensitive indication of the rela-

tive anisotropy of H_{c1} , which is itself only 1% of H_{c1} (i.e., we observe a small experimental discrepancy in the magnitude of a 1% effect).

As verification of the applied-field dependence predicted by Eqs. (5) and (6), the misalignment angle was measured for fields aligned along the [113] CL axis, a direction which is near to that of maximum misalignment. These results are shown in Fig. 8 and are compared with the relation $\Delta\psi H_a = 863$ deg Oe, obtained from $\Delta\psi$ fit of Eq. (9), and given by the heavy line in the IMS of Fig. 8. The equilibrium result of Eq. (9) lies between the experimental data for different field histories. Again, the hysteretic effect is probably due to weak pinning and the fact that the equilibrium FLL tends to rotate within the sample when the field is swept, owing to the field dependence of the equilibrium misalignment angle. This latter observation is corroborated by the experimental data in the mixed state, where both the misalignment angle and the hysteresis decrease at higher fields.

The constant IMS value depicted by the light line is the mean product $\Delta\psi H_a$. In the mixed state, the curve is simply drawn as a guide, except at $H_a = H_2$, where Eq. (6) was used to calculate the mixed-state slope,

$$\left. \frac{d(\Delta\psi H_a)}{dH_a} \right|_{H_2} = \left(\frac{8\pi C_L/B_0^2}{1 + 8\pi C_L/B_0^2} \right) \frac{dB_0/d\alpha}{B_0} \quad (10)$$

For this, we used the experimentally determined B_0 anisotropy from Eq. (8), and the measured FLL compressibility modulus

$$C_L = \frac{B_0^2}{8\pi} \left[3 \left(\frac{dB}{dH_a} \right)^{-1} - 1 \right] = (B_0^2/4\pi) dH/dB$$

found from Fig. 8 of I.

The quantity C_L can also be determined by DCSANS from the linear applied-field dependence of

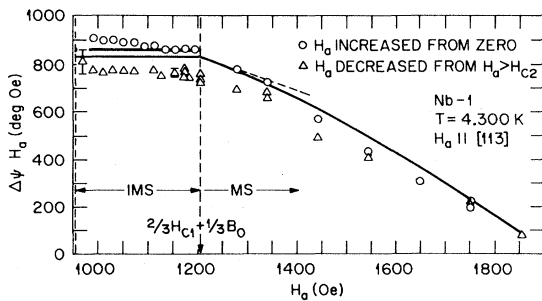


FIG. 8. Magnetic-field-intensity dependence of the misalignment angle for the field parallel to a [113] CL axis. The heavy solid line represents the expected value of $\Delta\psi H_a$ in the IMS. The curve in the mixed state is drawn as a guide, but the slope of the dashed line is related to the B_0 anisotropy and the FLL compressibility modulus through Eq. (10).

the flux density per unit cell for H_a just above H_2 [see Fig. 5(a)]. The value $C_L = 1.115 \pm 0.15 \times 10^4$ erg/cm³ found at 4.30 K by DCSANS agrees with that of the dM/dH_a measurements to within the experimental error; however, we have used the dM/dH_a results in Eq. (10) because those direct measurements of the slope appear to be more precise. As pointed out in I, no anisotropy in C_L could be resolved by either experimental technique. The result of Eq. (10) is plotted as a dashed line in Fig. 8, and is seen to depict the low-field mixed-state data within the range of experimental error. A quantitative comparison at higher fields must await a complete theory of mixed-state anisotropy.

In Sec. I we noted that the orientation-dependent Gibbs potential implies that a torque is exerted on the sample when a uniform field is aligned off a high-symmetry CL axis. In the IMS, the torque density is given by

$$\tau = - \frac{B dH_{c1}/d\alpha}{4\pi} \quad (11)$$

Although there have been no direct torque measurements performed on the present sample, Eq. (11) can be used for comparison with the recent torque determinations on niobium by Schneider, Schelten, and Heiden (SSH),¹⁹ and by Holzhäuser.²⁰ SSH measured the torque for field directions in the (110) plane, transverse to the axis of a cylindrical sample. Holzhäuser used the same sample geometry, and included measurements in the (100) plane. For these latter experiments, the samples were fabricated from ultrapurified niobium.²¹ Comparison of the present misalignment data with the mixed-state torque density measurements of SSH's Fig. 3 and Holzhäuser's Figs. 4 and 5 reveals agreement among the three experiments to a few percent with respect to the general features of the torque (i.e., positions of extrema and relative functional dependence). A complete quantitative comparison is difficult, since the workers present results in differing field and temperature regimes. However, assuming that the effective demagnetizing coefficient for those experimental geometries is $D \approx 0.5$, Eq. (11) can be compared to some specific reported data at $T = 4.2$ K in the (110) plane at $\alpha \approx 30^\circ$ (SSH), and at $\alpha = 36^\circ$ and $\alpha = 69^\circ$ (Holzhäuser) (using the present orientation-angle convention). This comparison indicates that Holzhäuser's results under equivalent conditions are systematically 10–20% larger than the present $\Delta\psi$ data. SSH present their data in the form of derived misalignment angles, $\epsilon(M, H)$ between the magnetization and the effective field, and $\epsilon(B, H)$ between the flux density and effective field. There is apparently a discrepancy in the calculation of these two quantities, which appear in Fig. 5 of SSH, since their consistency would require an unreasonably large $H_{c1} \approx 1670$ Oe at 4.2 K. Using the present value

axis is isosceles, such that net fourfold symmetry is achieved.

Idealized, the set of FLL neighbor directions that lie close to the $[1\bar{1}0]$ axis (i.e., for fields parallel to $[113]$ through $[110]$) would actually lie on the $[1\bar{1}0]$ axis were it not for small geometrical errors of about $\pm 2^\circ$ in the alignment of the sample in the field.

Figure 11 shows how the FLL also evolves into two coexisting orientation domains as the field is applied parallel to various CL axes in a (100) plane. In this case, the second domain is generated by reflection about the axis \bar{u} , which marks the intersection of the (100) CL plane with a plane orthogonal to the applied field. Here, $OA'B'$ and $OA''B''$ are the isosceles half cells representing the two FLL domains which, together, satisfy fourfold symmetry when the field is parallel to a $[001]$ axis.

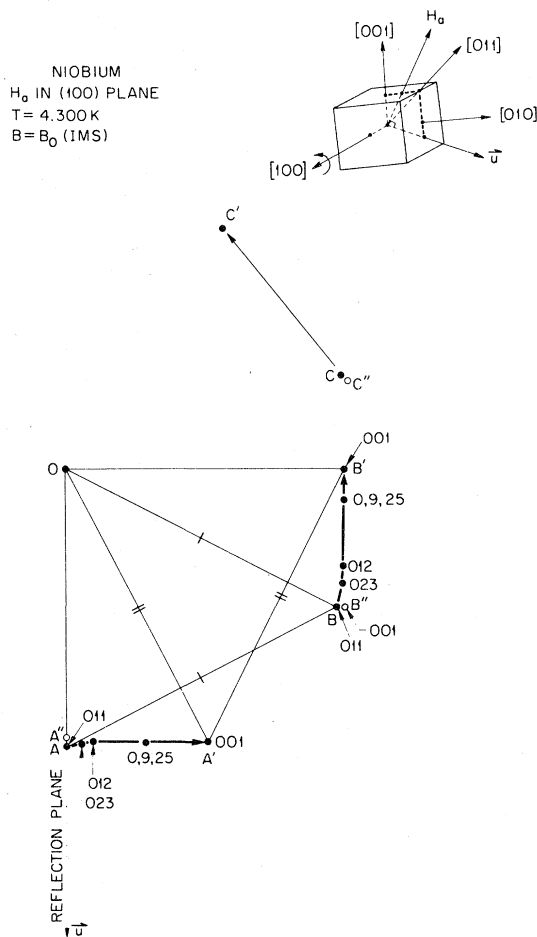


FIG. 11. Progressive change in the FLL morphology as the applied-field directions are varied in a (100) plane. Coexistence of lattice domains, generated by reflection about the axis \bar{u} , is required to preserve the twofold symmetry. $OA'B'$ and $OA''B''$ are the two isosceles FLL domains when H_a is parallel to a $[001]$.

For those CL directions where FLL domains of more than one orientation coexist, the FLL structure appears to be less stable than for those CL directions which possess only one domain. This phenomenon is displayed in Fig. 12, which is a plot of the FLL relative rocking-curve widths. These widths are obtained from the scattered neutron intensities as the sample is rotated through an angle ϕ about a vertical axis, as described in Sec. II. It is seen that broad rocking curves, indicative of a lattice less perfect in its angular orientation, systematically pervade for the CL directions showing two domains. Qualitatively, the CL orientations for which the rocking-curve widths peak sharply are observed to be those where the FLL neighbor directions change most rapidly with CL orientation in the field. This may account for the wide range of rocking-curve widths obtained for newly produced FLL at those CL orientations. The experimental error in $\Delta\phi$ for a given FLL is denoted by the error bar, for example, on the single determination at $\alpha \approx 8^\circ$ in the $(1\bar{1}0)$ plane.

From a theoretical point of view, the rocking-curve widths should reflect the strength of the restoring force, at the free-energy minimum, with respect to variations of the three parameters that are, in general, required to specify the orientation and symmetry of the FLL in the host crystal.¹⁰ These features may be very sensitive manifestations of the small anisotropies of the superconductive system. For example, at lower temperatures $T \leq 2\text{ K}$, we observe two domains of square FLL for applied fields parallel to a $\langle 001 \rangle$ in the IMS. These domains each had nearest-neighbor directions being 30° from CL $\langle 110 \rangle$ axes. Other workers have observed these results under similar conditions, and in addition have reported nearest-neighbor directions parallel to a $\langle 110 \rangle$ and $\langle 100 \rangle$.^{14,28} These combined results imply that at least four separate square FLL are stable in pure niobium at low temperatures.

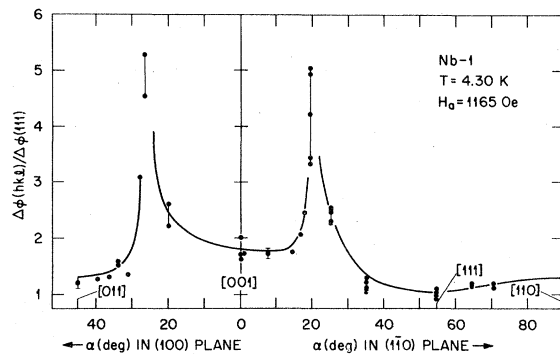


FIG. 12. Relative rocking-curve widths of the FLL in the IMS for the vertical field geometry [see Fig. 2(a)]. The applied field is parallel to CL directions $[hkl]$ in the $(1\bar{1}0)$ and (100) planes. The data are normalized to the width $\Delta\phi(111)$, the case where \bar{H}_a is parallel to a $[111]$ CL axis.

These observations can be reconciled by imagining the possibility of several free-energy potential minima with respect to the orientation of a (square) FLL, when the applied field is along a CL fourfold axis. The disposition of those minima would be such as to preserve the required fourfold symmetry. The FLL orientation observed in a particular experiment would depend upon the potential minima (not necessarily absolute) sites of initial nucleation, and the kinetics of FLL growth. In this view, it is possible experimentally to observe a situation in which some domains are absent. This phenomenon was, in fact, observed on occasion during the course of the present measurements.

A semiquantitative theoretical description of the expected FLL morphology at low temperatures and low fields has been given by Fischer and Teichler.¹² Their calculations stem from the asymptotic form of the attractive fluxoid interaction, and predict only $\langle 110 \rangle$ nearest-neighbor directions for a square FLL in niobium. In reality, of course, fluxoids in a type-II/1 superconductor are never widely separated, and the details of the anisotropic interaction in the range of strongest attraction must be calculated to give a rigorous description. This latter type of analysis, accounting for effects of Fermi-surface anisotropy, is currently in progress within the context of the boson theory.²⁹ However, the preliminary results, considering only nearest-neighbor forces at $T=0$, concur with Fischer and Teichler, and fail to predict quantitatively the existence of multiple FLL orientation domains. A more detailed analysis, and extension to finite temperature, is in progress.¹⁶

Schelten *et al.*²⁸ observed a low-temperature transformation from the square FLL to two distorted triangular half cells as the field was increased along a fourfold-CL axis. The present measurements confirm this result, finding the near-neighbor directions of the triangular half cells to be near $\langle 001 \rangle$ axes.

The details of the low-field temperature dependence of the FLL symmetry are given in Figs. 13(a) and (b), for the fourfold case. Together, these figures reveal that for $T \geq 4$ K, the FLL half cells for each domain are isosceles triangles, the symmetry of which approaches the equilateral case as $T \rightarrow T_c$. This is anticipated on theoretical grounds due to the vanishing of anisotropic effects near T_c .⁹ Below about 4 K, the half cell domains distort, but in such a way that the area of the basic cell is nearly the same as that of a square lattice with the same nearest-neighbor distance. Finally at $T \leq 2$ K, a structural transition can occur, which results in the two domains of square FLL discussed above. We observed no progressive transformation from the distorted triangular to the square FLL, nor evidence for their coexistence. Rather, the data imply an abrupt structural transition.

As noted previously, the applied-field dependence

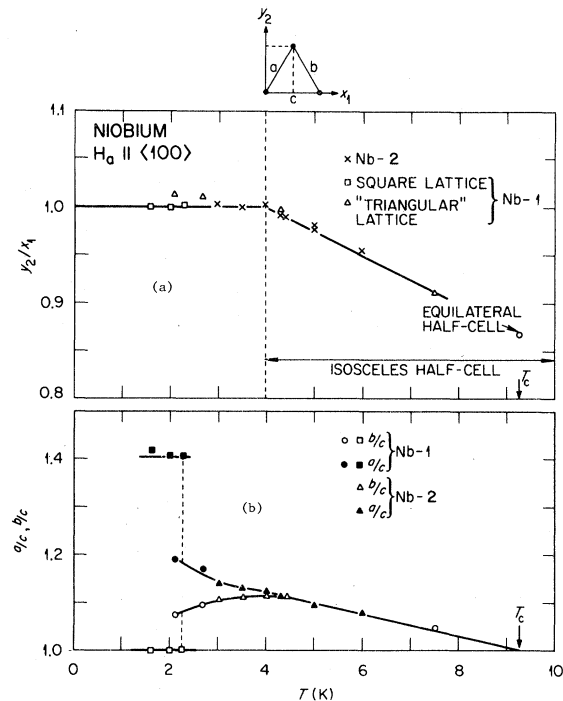


FIG. 13. Temperature dependence of the FLL half cell symmetry for fields in the IMS, and parallel to a CL $[100]$ axis. (a) The ratio of height to base shows that: (i) below $T \approx 4$ K the triangular FLL unit cell has same area as a square with the same nearest-neighbor separation; (ii) as T increases above ~ 4 K, the symmetry progresses toward an equilateral half cell at T_c . (b) The ratios of side lengths to base of the triangular half cell shows that: (i) for $T \geq 4$ K the half cell is isosceles; (ii) below approximately 4 K the half cell distorts; (iii) a structural transition from a distorted triangular half cell to a square FLL occurs near 2 K.

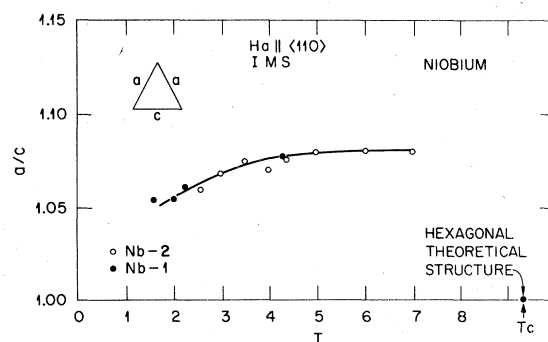


FIG. 14. Temperature dependence of the FLL symmetry for H_a parallel to a CL $\langle 110 \rangle$. The side-to-base ratio of the isosceles half cell shows a decrease at low temperatures, and there is no sign of evolution to a hexagonal FLL for temperatures to 7 K.

$H_a \parallel$	H. TEICHLER (LOW FIELD)	TAKANAKA - ROGER, DELRIEU (HIGH FIELD)	BOSON THEORY (LOW FIELD) $T=0$	PREVIOUS EXPERIMENTS	PRESENT RESULTS
$\bar{1}\bar{1}\bar{1}$					
$\bar{1}\bar{1}0$					
$\bar{1}\bar{1}2$					
001					

FIG. 15. Pictorial summary of the theories of Teichler (Ref. 12), DRK (Ref. 10), and the boson model (Ref. 29), and the currently available experimental results (given in Ref. 5). (For clarity, not all of the experimentally observed square FLL domains are shown; see Sec. III D).

of the FLL symmetry is weak for CL axes between $[113]$ and $[110]$ in the $(\bar{1}\bar{1}0)$ plane. This is true also of the temperature dependence for these orientations. However, some distinguishing features exist in regard to the case for H_a parallel to a CL $\langle 110 \rangle$, which is shown in Fig. 14. The DRK models predict a half cell shape parameter which is too large ($a/c = 1.15$), and which increases as $T \rightarrow 0$, in contradiction with the present measurements. The preliminary $T=0$ results of the boson theory,²⁹ on the other hand, predict a shape parameter which is less than unity (i.e., presumably the FLL passes through hexagonal symmetry at some $T > 0$). At higher temperatures, up to ~ 7 K, there is no experimental evidence for damping of the shape anisotropy, which, theoretically, should result in a hexagonal FLL at T_c . Obviously, there is need to extend the measurements to the more difficult ranges of both higher and lower temperatures as the theoretical descriptions improve.

A pictorial summary of the most realistic theoretical models, and the available experimental observations are presented in Fig. 15.

IV. SUMMARY

The features of the H_{c1} anisotropy in a single-crystal niobium sphere have been determined using a

double-crystal small-angle neutron-scattering technique. The orientation dependence can be satisfactorily described by an expression using two cubic-harmonic terms, and, at $T = 4.30$ K, displays a maximum relative anisotropy of about 1%. The results are shown to be consistent with the dM/dH_a measurements of the previous paper,¹ and with the present direct measurements of the misalignment angle between the fluxoid axes and the applied field in the intermediate mixed state. In addition, the anisotropy is in semiquantitative accord with previous torque determinations.^{19,20} However, the present results are at variance with the recent experimental data of Ohta and Ohtsuka,¹⁷ and the origin of this discrepancy is unresolved.

Orientation-dependent measurements of B_0 revealed a maximum relative anisotropy of about 2% between 4.30 and 1.6 K, and detailed measurements at 4.30 K showed the data could be fit to a two-cubic-harmonic series. These results disagree with the only other known experimental study of B_0 anisotropy in niobium,¹⁸ for reasons that are not completely clear.

Fundamental theoretical descriptions of these low-field anisotropic phenomena are scant. The qualitative features of the H_{c1} anisotropy calculated near T_c by Takanaka and Hubert¹⁵ is in accord with the five experiments mentioned above. On the other hand,

at $T=0$, the preliminary results of the boson theory provide qualitative agreement with both the present H_{c1} and B_0 measurements.

The FLL-CL symmetry correlations have been mapped progressively, for several CL orientations at fixed temperature in the IMS, and as a function of temperature for some specific high-symmetry directions. These results, along with the previous experimental data,^{10,11,14,28} reveal that the present theories^{9-12,29} are unable to describe the situation at low fields completely. The multiple-orientation-domain effects, and rapid variation of FLL morphology with CL orientation, are probably the most sensitive of the low-field anisotropic superconducting properties.

It is hoped that the experimental evidence presented herein, along with the questions raised, will serve as added stimulus for the development of more complete theoretical descriptions of these orientation-

dependent superconducting parameters.

Note added in proof. Since submission of this paper, we have become aware of new results, both experimental³⁰ and theoretical,^{31,32} involving the anisotropies in H_{c1} and B_0 . These works verify semiquantitatively the sense and magnitude of the anisotropies reported here, and confirm the validity of the expression used for the analysis.

ACKNOWLEDGMENTS

In addition to those acknowledged in the previous paper, the authors would like to thank Alan Pringle and Richard Harper for valuable assistance with the neutron-diffraction experiments. This research was sponsored by the Division of Materials Science, U. S. DOE under Contract No. W-7405-eng-26 with the Union Carbide Corporation.

*Guest Scientist from Département de la Recherche Fondamentale, Centre d'Etudes Nucléaires, Grenoble, France.

- ¹H. R. Kerchner, D. K. Christen, and S. T. Sekula, *Phys. Rev. B* **21**, 86 (1980) (preceding paper).
²D. K. Christen, F. Tasset, S. Spooner, and H. A. Mook, *Phys. Rev. B* **15**, 4506 (1977).
³D. K. Christen, S. Spooner, P. Thorel, and H. R. Kerchner, *J. Appl. Cryst.* **11**, 650 (1978).
⁴D. K. Christen and P. Thorel, *Phys. Rev. Lett.* **42**, 191 (1979).
⁵A review of the previous work in this field is given by J. Schelten, in *Anisotropy Effects in Type-II Superconductors*, edited by H. W. Weber (Plenum, New York, 1977), p. 113.
⁶P. Thorel and D. K. Christen, *J. Appl. Cryst.* **11**, 654 (1978).
⁷A summary of IMS domain properties as studied by electron microscopy is given by C. Obst, in Ref. 5, p. 139.
⁸D. K. Christen (unpublished).
⁹K. Takanaka, *Prog. Theor. Phys.* **46**, 357, 1301 (1971); and **49**, 64 (1973).
¹⁰M. Roger, thesis (Orsay, 1974) (unpublished); R. Kahn, Ph.D. thesis (Orsay, 1977) (unpublished).
¹¹M. Roger, R. Kahn, and J. M. Delrieu, *Phys. Lett. A* **50**, 291 (1974).
¹²K. Fischer and H. Teichler, *Phys. Lett. A* **58**, 402 (1976); H. Teichler, in Ref. 5, p. 65.
¹³J. Schelten, H. Ullmaier, and G. Lippman, *Z. Phys.* **253**, 219 (1972).

- ¹⁴U. Essmann, *Phys. Lett. A* **41**, 477 (1972).
¹⁵K. Takanaka and A. Hubert, in *Proceedings of the Fourteenth International Conference on Low Temperature Physics*, edited by M. Krusius and M. Vuorio (American Elsevier, New York, 1975), Vol. II, p. 309.
¹⁶H. Umezawa and M. Tachiki (private communication).
¹⁷N. Ohta and T. Ohtsuka, *J. Phys. Soc. Jpn.* **45**, 59 (1978).
¹⁸C. E. Gough, in Ref. 5, p. 79.
¹⁹R. Schneider, J. Schelten, and C. Heiden, in Ref. 5, p. 177.
²⁰W. Holzhäuser, *J. Low Temp. Phys.* **24**, 175 (1976).
²¹N. Ye. Alekseyevskiy, V. I. Nizhankovskiy, and K. -H. Bertel, *Fiz. Metal. Metalloved.* **37**, 63 (1974) [*Phys. Met. Metallogr.* **37**, 53 (1974)].
²²Y. Wada and Y. Tamura, *Prog. Theor. Phys.* **50**, 1194 (1973).
²³Y. Tamura and Y. Wada, *Prog. Theor. Phys.* **51**, 43 (1974).
²⁴Y. Tamura, *Prog. Theor. Phys.* **51**, 315 (1974).
²⁵J. Matricon, *Phys. Lett.* **9**, 289 (1964).
²⁶A. L. Fetter, *Phys. Rev.* **147**, 153 (1966).
²⁷E. H. Brandt, *Phys. Status Solidi B* **51**, 345 (1972).
²⁸J. Schelten, G. Lippmann, and H. Ullmaier, *J. Low Temp. Phys.* **14**, 213 (1974).
²⁹T. Koyama, M. Tachiki, H. Matsumoto, and H. Umezawa, *Phys. Rev. B* **20**, 918 (1979).
³⁰H. Kiessig, U. Essmann, and W. Wiethaup, *Phys. Lett. A* **71**, 467 (1979).
³¹K. Takanaka (unpublished).
³²Kenji Takanaka and Tomitaro Nagashima (unpublished).